Translational Oncology
www.transonc.com

Volume 12 Number 3 March 2019 pp. 404–416 404

Cyclical Treatment of Colorectal Tumor Spheroids Induces Resistance to MEK Inhibitors

Pradip Shahi Thakuri[*], Gary D. Luker[†,‡,§] and Hossein Tavana[*]

[*]Department of Biomedical Engineering, The University of Akron, Akron, OH 44325, USA; [†]Department of Radiology, University of Michigan, Ann Arbor, MI 48105, USA; [‡]Department of Microbiology and Immunology, University of Michigan, Ann Arbor, MI 48105, USA; [§]Department of Biomedical Engineering, University of Michigan, Ann Arbor, MI 48105, USA

Abstract

Adaptive drug resistance is a major obstacle to successful treatment of colorectal cancers. Physiologic tumor models of drug resistance are crucial to understand mechanisms of treatment failure and improve therapy by developing new therapeutics and treatment strategies. Using our aqueous two-phase system microtechnology, we developed colorectal tumor spheroids and periodically treated them with sub-lethal concentrations of three Mitogen Activated Kinase inhibitors (MEKi) used in clinical trials. We used long-term, periodic treatment and recovery of spheroids to mimic cycles of clinical chemotherapy and implemented a growth rate metric to quantitatively assess efficacy of the MEKi during treatment. Our results showed that efficacy of the MEKi significantly reduced with increased treatment cycles. Using a comprehensive molecular analysis, we established that resistance of colorectal tumor spheroids to the MEKi developed through activation of the PI3K/AKT/mTOR pathway. We also showed that other potential feedback mechanisms, such as STAT3 activation or amplified B-RAF, did not account for resistance to the MEKi. We combined each of the three MEKi with a PI3K/mTOR inhibitor and showed that the combination treatments synergistically blocked resistance to the MEKi. Importantly, and unlike the individual inhibitors, we demonstrated that synergistic concentrations of combinations of MEK and PI3K/mTOR inhibitors effectively inhibited growth of colorectal tumor spheroids in long-term treatments. This proof-of-concept study to model treatment-induced drug resistance of cancer cells using 3D cultures offers a unique approach to identify underlying molecular mechanisms and develop effective treatments.

Translational Oncology (2019) 12, 404–416

Introduction

Preclinical studies are essential to cancer drug discovery. Historically, these studies have been carried out primarily using two-dimensional (2D) cell cultures and then validated in animal models. However, 2D cultures lack key morphological and biological properties of human tumors. The use of 2D cultures is thought to be a major contributing factor to the high attrition rate of drug candidates in animal studies and failures in clinical trials [1]. To address this problem, 3D cultures of cancer cells as tumor spheroids have been used in cancer research because they resemble both the morphology and biologic characteristics of solid tumors [2–4]. Despite increasing use of spheroids for compound screening to identify effective drugs, their potential to study cancer drug resistance remains underexplored. Major barriers include difficulties with long-term culture and periodic drug treatment of spheroids, intense labor associated with handling the cultures, and quantitative analysis of drug responses of cancer cells in spheroid cultures [2]. Here, we addressed these challenges and demonstrated the utility of tumor spheroids to model resistance to

Address all correspondence to: Hossein Tavana, Ph.D., P. Eng., 260 S. Forge St., Akron, OH 44325.
E-mail: tavana@uakron.edu
Received 5 October 2018; Revised 19 November 2018; Accepted 19 November 2018

1936-5233/19
https://doi.org/10.1016/j.tranon.2018.11.009

molecular inhibitors and explore the underlying molecular mechanisms.

Colorectal cancer is the third leading cause of cancer death in men and women in the United States [5]. Approximately, 30–40% of colorectal cancers have KRAS mutations, 10–15% contain B-RAF mutations, and 10–20% have an activating PIK3CA mutation [6–8]. These mutations cause aberrant activities of oncogenic pathways RAS/RAF/MEK/ERK (MAPK) and PI3K/AKT/mTOR. As such, these pathways present attractive therapeutic targets. Several studies showed that specific molecular inhibitors of MEK and RAF (MEKi and RAFi) suppressed growth of colorectal tumors in vivo [9,10]. Nevertheless, colorectal cancer cells often show resistance to these inhibitors by activating other signaling pathways such as PI3K/AKT/mTOR or JAK/STAT to mediate resistance to MEKi [11]. Feedback activation of receptor tyrosine kinases (RTKs) such as epidermal growth factor receptor (EGFR) causes resistance to RAFi [12]. Alternatively, continuous exposure to a MEKi may lead to mutation of MEK [13], while resistance to continuous exposure to RAFi may occur through amplification of B-RAF or other components of the MAPK pathway [14,15]. Therefore, understanding mechanisms of drug resistance and developing strategies to overcome them is crucial to improve colorectal cancer treatments.

To model drug resistance of colorectal cancer, we used our robotic, aqueous two-phase system technology to generate tumor spheroids of colorectal cancer cells harboring B-RAF and PIK3CA mutations. Using a pulsed-dosing regimen to mimic intermittent cycles of chemotherapy administered to patients, we cyclically treated tumor spheroids with three MEKi, as demonstrated before [16]. The pulsed-dosing strategy has shown advantages over continuous drug administration by producing prolonged anti-tumor activity in vivo [17,18]. The pulsed dosing strategy using the BRAF inhibitor, vemurafenib, delayed acquired resistance in a melanoma mouse model [19]. This dosing regimen approach has also been adopted in clinical trials of targeted therapies against colorectal cancer [20]. We quantitatively compared efficacies of MEKi based on normalized growth rates of spheroids after each cycle of treatment. Our results clearly showed that effectiveness of each MEKi to suppress growth of tumor spheroids significantly reduced during successive treatment cycles. Our molecular analysis showed that repeated exposure of colorectal tumor spheroids to a MEKi significantly upregulated AKT activity without affecting other possible mediators of resistance, such as STAT3 and B-RAF. We also demonstrated that combination treatments of MEK and PI3K inhibitors synergistically inhibited growth of tumor spheroids during long-term cycles of treatment and recovery and downregulated signaling through these pathways. Importantly, this proof-of-concept study using cyclical treatment of tumor spheroids reproduced adaptive drug resistance of cancer cells due to feedback signaling of kinase pathways known from animal studies. Our study presents a unique approach to identify mechanisms of drug resistance and evaluate rationale therapeutic interventions to overcome resistance in 3D tumor models of cell lines with different genetic backgrounds and with patient-derived cells.

Materials and Methods

Cell Culture

Mc Coy's 5A medium (Sigma) was used to culture HT-29 (ATCC) and HCT116 (ATCC) colorectal cancer cells. The medium was supplemented with 10% fetal bovine serum (FBS) (Sigma), 1% Streptomycin/Penicillin (Thermo Fisher Scientific), and 1% glutamine (Thermo Fisher Scientific). Cells were cultured in a humidified incubator at 37 °C and 5% CO2. Cells were dissociated from 80–90% confluent monolayer cultures in tissue culture flasks using 0.25% trypsin (Thermo Fisher Scientific). Trypsin was neutralized using the complete growth medium. The cell suspension was centrifuged down at 1000 rpm for 5 min. After removing the supernatant, cells were suspended in 1 ml of the culture medium and counted using a hemocytometer prior to spheroid formation.

Spheroid Formation

A polymeric aqueous two-phase system was used to form colorectal tumor spheroids. Bio-ultra polyethylene glycol (PEG) with a molecular weight of 35 kDa (Sigma) and dextran (DEX) with a molecular weight of 500 kDa (Pharmacosmos) were dissolved in the complete growth medium to obtain solutions with concentrations of 5.0% (w/v) PEG and 12.8% (w/v) DEX. A round-bottom ultralow attachment 384-well plate (Corning) was used as the "destination plate". Each well of this plate was loaded with 30 μL of the aqueous PEG phase medium. A suspension of 1×10^8 cells/mL was prepared and 100 μL of the suspension was thoroughly mixed with 100 μL of the 12.8% (w/v) aqueous DEX phase medium. This reduced the concentration of the DEX polymer to 6.4% (w/v) and adjusted the density of cells to 5×10^7 cells/mL. Each well from one column of a flat-bottom 384-well plate (Corning), which was used as the "source plate," was loaded with 25 μL of the resulting cell suspension in the DEX phase medium. A robotic liquid handler, Bravo SRT (Agilent Technologies), was used to aspirate 0.3 μL of the suspension containing 1.5×10^4 cells from each well and dispense it into each well of the destination plate containing the aqueous PEG phase. This aspiration and dispensing process was done column by column. Uniformity of the high-density cell suspension in the source plate was maintained by robotically mixing the content of the wells prior to each aspiration step. The destination plate was incubated for 48 hours to allow cells in each well aggregate into a compact spheroid.

Preparing Drug Solutions

Trametinib, PD0325901, selumetinib, sorafenib, AZ628, GDC0994, ulixertinib, dactolisib, PI-103, GSK1059615, and pictilisib were purchased from Selleckchem (Houston, TX). Stock solutions of these molecular inhibitors were prepared according to the manufacturer's instructions. Except for dactolisib that was dissolved in dimethylformamide, other compounds were dissolved in dimethyl sulfoxide (DMSO). Stock solutions of the inhibitors were stored in –80 °C. The inhibitors were tested against tumor spheroids according to the protocol we described previously [21,22].

Cyclical Treatment of Spheroids with Inhibitors and Recovery from Treatment

Sub-lethal concentrations of trametinib (5 nM), PD0325901 (100 nM), and selumetinib (100 nM) were selected based on dose-dependent drug tests against HT-29 spheroids. We selected these concentrations to produce growth inhibition in HT-29 tumor spheroids. Spheroids were subjected to three rounds of drug treatment separated by two rounds of recovery phases. The three rounds of treatment were designated as Round1, Round2, and Round3. The recovery periods were designated as Recovery1 and

Recovery2. Each phase lasted 6 days. Each treatment phase included drug addition to spheroids at the beginning and drug renewal 72 hours later, whereas each recovery phase included culture medium addition to spheroids at the beginning and culture medium renewal 72 hours later. Concentration of each drug was maintained constant during all three treatment phases.

Concentrations of 10 nM trametinib, 200 nM PD0325901, and 200 nM selumetinib were prepared by serially diluting their respective stock solutions in the culture medium. These solutions were prepared twice the final concentrations for testing against colorectal tumor spheroids. Next, 30 μL from each of these drug solutions was added to each well of the destination plate that contained a spheroid in the DEX phase drop immersed in 30 μL of the aqueous PEG phase. This addition diluted concentrations of PEG and DEX, converting the two-phase system to a single medium phase containing trace amounts of the polymers. It also reduced drug concentrations to 5 nM trametinib, 100 nM PD0325901, and 100 nM selumetinib. After 72 hours, 30 μL of each drug solution at its working concentration was added to the corresponding wells. At the end of Round1, the culture medium containing the inhibitors was robotically aspirated out of the microwells. Next, to start the Recovery phase, 30 μL of fresh medium was added to the wells containing the spheroids. Another 30 μL of fresh medium was added 72 hours later. At the end of Recovery1, half of the medium was carefully aspirated from each well. The Round2 treatment was initiated by adding a drug solution containing 2× concentration of each inhibitor in 30 μL of the medium, and renewal was done by adding 30 μL of each drug solution at 1× concentration after 72 hours. In parallel, 30 μl of fresh medium was added to spheroids from Recovery1, and 30 μl fresh medium was renewed after 72 hours. These spheroids that were grown in the medium were used as the non-treated group for the Round2 treatment. At the end of Round2, drug solutions were removed from the wells and the Recovery2 phase was initiated. This was followed by another round of treatment (Round3) that was initiated by adding a drug solution containing 2× the concentration of each inhibitor in 30 μL of the medium, and renewed by adding 30 μL of each inhibitor at 1× concentration after 72 hours. In parallel, 30 μl of fresh medium was added to spheroids from Recovery 2, and 30 μl of fresh medium was renewed after 72 hours. These spheroids that were grown in the medium were used as the non-treated group for the Round3 treatment.

Dose-Dependent Cyclical Treatments of Spheroids with MEKi and Recovery from Treatments

To compare dose responses of spheroids to the MEKi, spheroids were assigned into two groups. Spheroids of the first group were treated with each inhibitor, i.e., 5 nM trametinib, 100 nM PD0325901, and 100 nM selumetinib, followed by a recovery phase. The experimental protocol for Round1 and Recovery1 phases was described above. Then, the recovered spheroids were treated with different concentrations of the inhibitors during treatment Round2, i.e., 0.25 × IC_{50}, 0.5 × IC_{50}, 1 × IC_{50}, 2 × IC_{50}, and 4 × IC_{50} of the MEKi. IC_{50} values of the three MEKi are listed in the Supplemental Table S3. To initiate the treatment Round2, the volume of the medium in microwells was measured, and the solution of each MEKi at twice the desired concentrations was added to wells. The treatments were renewed by adding each inhibitor solution at a 1× concentration in 30 μL of the medium after 72 hours. On the other hand, spheroids in the second group were treated only once with each of the MEKi at 0.25 × IC_{50}, 0.5 × IC_{50}, 1 × IC_{50}, 2 × IC_{50}, and 4 × IC_{50} concentrations during Round1. The effects of dose-dependent treatments on spheroids from the two groups were quantitatively compared as described below.

Analysis of Growth of Spheroids to Quantify Drug Resistance

Prior to the start of experiments and at the end of each cycle of treatment and recovery, phase images of spheroids were captured using an inverted microscope (Axio Observer, Zeiss) equipped with a high-resolution camera (AxioCam MRM, Zeiss). The images were analyzed using ImageJ software (NIH) to measure the diameter of spheroids. The volume of spheroids was determined from the diameter data assuming a spherical shape for spheroids. The inhibitor concentration, c, and the treatment and recovery time, t = 6 days, were the same during each round. A growth rate parameter (k_c) was calculated for spheroids that were treated with a MEKi by finding the difference in the volume of spheroids at the end and beginning of each round of treatment. Similarly, the growth rate (k_0) was calculated for spheroids that were not treated with MEKi but cultured in the medium by finding the difference in the volume of spheroids at the end and beginning of each round. A normalized growth rate parameter was found by dividing the growth rate of treated spheroids by the growth rate of untreated spheroids, i.e., k_c/k_0, to quantify resistance. Experiments for each condition used n = 14 spheroids. Statistical analysis was performed using student's *t*-test in Microsoft Excel and considering a significance level of $p < 0.05$ between the treatment groups.

Similarly, we calculated the growth rate of spheroids for the two groups of spheroids treated with different concentrations of each MEKi described above. The growth rates of spheroids at five different treatment concentrations, i.e., k_n*IC_{50}, where n = 0.25, 0.5, 1, 2, and 4, were calculated by subtracting the volumes of spheroids measured at the beginning and end of treatments. Similarly, the growth rate of untreated spheroids (k_0) was calculated by subtracting the volume of untreated spheroids measured at the beginning and end of each round. A normalized growth rate parameter was computed by dividing the growth rate of treated spheroids by the growth rate of untreated spheroids, i.e., k_c/k_0, to quantify resistance. Furthermore, a parametric approach using area under the dose response curve (AUC) was employed to quantify the resistance to the MEKi [21]. Experiments for each condition used n = 7 spheroids. Statistical analysis was performed using student's *t*-test in Microsoft Excel and considering a significance level of $p < 0.05$ between the two treatment groups.

Western Blotting

For all Western blot experiments, spheroids were harvested from 384-well plates after treatment and transferred into 50 ml conical tubes. After centrifugation and removing of the supernatant, spheroids were washed with PBS, and lysed in 500 μL of complete RIPA buffer (50 mM Tris–HCl, 150 mM NaCl, 1% NP-40, 0.5% sodium deoxycholate, and 0.1% SDS, pH 7.4 ± 0.2) with protease inhibitor (complete mini, Roche Diagnostics) and phosphatase inhibitor (Thermo Fisher Scientific). To ensure complete lysis, spheroids were sonicated (Vibra-Cell, Sonics) twice for 5 s at a 20% amplitude level. Total protein concentration was determined using a BCA quantification assay kit (Thermo Fisher Scientific). Then, 10–20 μg of the protein solution was loaded onto a 4–15% gel (Bio-Rad) for electrophoresis and the gel was transferred onto a

nitrocellulose membrane by electroblotting. Membranes were blocked with 5% BSA (Sigma) for 1 h. Primary antibodies for phospho-p44/42 MAPK (Erk1/2), p44/42 MAPK (Erk1/2), phospho-AKT (Ser473), AKT (pan) (C67E7), phospho-BRAF (Ser445), BRAF (D9T6S), phospho-STAT3 (Tyr705), and STAT3 (79D7) were purchased form Cell Signaling Technology. Solutions of primary antibodies were prepared at concentrations recommended by the manufacturer. Membranes were incubated overnight at 4 °C with primary antibody solutions. After repeated washing, membranes were incubated with a horseradish peroxidase (HRP)-conjugated secondary antibody for 1 h, followed by repeated washing. Detection was carried out using an ECL chemiluminescence detection kit (GE Health Care) and FluorChem E imaging system (ProteinSimple).

Short-Term Combination Treatments of Spheroids

Trametinib, PD0325901, and selumetinib were used in combination with dactolisib in separate experiments. The IC_{50} value for each inhibitor against HT-29 spheroids was obtained from its respective dose–response curve (Supplementary Table 3 (S3)). Each of the three MEKi and dactolisib were combined at fixed concentration ratios of multiples (0.25, 0.5, 1, 2, 4) of the respective IC_{50} values. Solutions with these concentrations were made by serially diluting the stock solutions in the culture medium. Each combination of concentrations for a pair of drugs used n = 14 replicates. In parallel to each combination treatment, spheroids of HT-29 cells were treated with the MEKi or dactolisib used as single agents. Next, PrestoBlue was added to wells and after incubating the spheroids for 4 hours, the fluorescence signal was measured with a plate reader (Synergy H1M, BioTek Instruments). Both control (non-treated) and drug-treated groups had n = 14 replicates. Viability of spheroids treated with each concentration of an inhibitor was normalized to that of non-treated spheroids and expressed as percent viability. GraphPad Prism 5 was used to fit a four-parameter sigmoidal dose–response curve to the viability data and to determine AUC. A combination index (CI) was used to determine synergism between combinations of the inhibitors.

Long-Term Cyclic Combination Drug Treatment/Recovery of Spheroids

Specific pairs of concentrations of each of the three MEKi and dactolisib that generated synergistic responses in HT-29 spheroids during Round1 treatment were selected for long-term experiments. These concentrations were $0.25 \times IC_{50}$ for trametinib/dactolisib, $0.25 \times IC_{50}$ for PD0325901/dactolisib, and $0.5 \times IC_{50}$ for selumetinib/dactolisib pairs. In parallel to each combination treatment, HT-29 spheroids were treated with the single-agent MEKi or dactolisib. The effectiveness of long-term treatment with each drug combination was assessed by comparing the growth inhibitory effects of the combination pair and each inhibitor used alone. The growth rates of spheroids under no treatment (vehicle control), single-agent treatments, and combination treatments were calculated by subtracting the volume of spheroids at the end of the 30-day treatment period and the volume of spheroids at the beginning. To calculate growth inhibitory effects at the end of day 30, the difference in growth rates of control spheroids (k_0) versus treated spheroids (k_c) were divided by k_0, i.e., Growth inhibition = $(k_0-k_c)/k_0$. One-way ANOVA was used to analyze the difference among the single-agent treatments, combination treatments, and vehicle control followed by a post-hoc Tukey test. The analysis was performed using Minitab (n = 7).

Results

Microprinting of Tumor Spheroids

The aqueous two-phase system (ATPS) microprinting approach effectively confined cancer cells in a DEX phase nanodrop to facilitate self-assembly into a compact spheroid within 48 hours in each well of 384-well plates (Figure 1, *A-C*) [23]. Immersion of the nanodrop within the aqueous PEG phase ensured diffusive influx of nutrients into the drop phase to nourish the cells and efflux of waste products of cells into the immersion phase [24]. Unlike several other cell printing/patterning techniques, this microprinting approach does not exert any mechanical, thermal, or chemical stresses on cells, producing spheroids containing fully viable cells [24]. Renewing the culture medium or adding a drug solution reduced concentrations of PEG and DEX polymers below a threshold required to maintain two separate phases (Figure 1*D*) [25]. Thus, this approach was solely used to conveniently micropattern spheroids and was not needed after spheroids formed. Medium exchanges every 72 hours ensured availability of fresh nutrients and removal of waste products of cells to support cellular metabolic activities. We have previously shown that our robotic spheroid technology generates consistently-sized spheroids that reproduce biologic properties of solid tumors [21,26].

Screening of Molecular Inhibitors Against Colorectal Tumor Spheroids

B-RAF and PIK3CA mutations in HT-29 cancer cells constitutively activate signaling through MAPK and PI3K pathways [27]. Targeting these oncogenic pathways has shown efficacy against colorectal cancer both in vitro and in vivo [28–30]. To identify effective inhibitors against these pathways in our model of drug resistance, we selected a panel of inhibitors of MAPK and PI3K pathways and screened them dose-dependently against the colorectal tumor spheroids. The list of the inhibitors and their molecular targets are given in Supplementary Tables 1 (S1) and 2 (S2). We compared effectiveness of the inhibitors based on area under the curve (AUC) analysis previously described [21]. The AUC value ranges from 0 to 1. An AUC value of 0 means 100% cell kill, whereas an AUC value of 1 indicates that all cells are viable. This analysis segregates compounds with low AUC values that are more effective from the less effective compounds with higher AUC values [21]. Among the inhibitors of MAPK (Figure 1, *E-F*) and PI3K (Figure 1, *G-H*) pathways, trametinib, PD0325901, and selumetinib received AUC scores of 0.33, 0.59, and 0.63, respectively, and ranked as the most effective compounds. This screening revealed that suppressing the MEK1/2 kinase in HT-29 spheroids most effectively inhibited growth. Thus, we selected these three MEKi to model acquired drug resistance of colorectal tumor spheroids.

Long-Term Cyclic Treatment of Spheroids with MEKi

To demonstrate treatment-induced resistance of colorectal cancer cells to MEKi, we determined effectiveness of the three MEKi against HT-29 spheroids for three six-day cycles of treatment separated by six-day recovery intervals (Figure 2*A*). We calculated the growth rate parameter, k_c, for drug-treated spheroids (Figure S1, *A-C*) and k_0 for control spheroids (Figure S1, *D-F*). Representative images of spheroids before drug treatments, and images of drug-treated and non-treated spheroids from different rounds are shown in Figure S1, *G-I*. The values for k_c and k_0 from different rounds are tabulated in Figure 2*B-D*. This resulted in average k_c/k_0 values of –0.1941, –

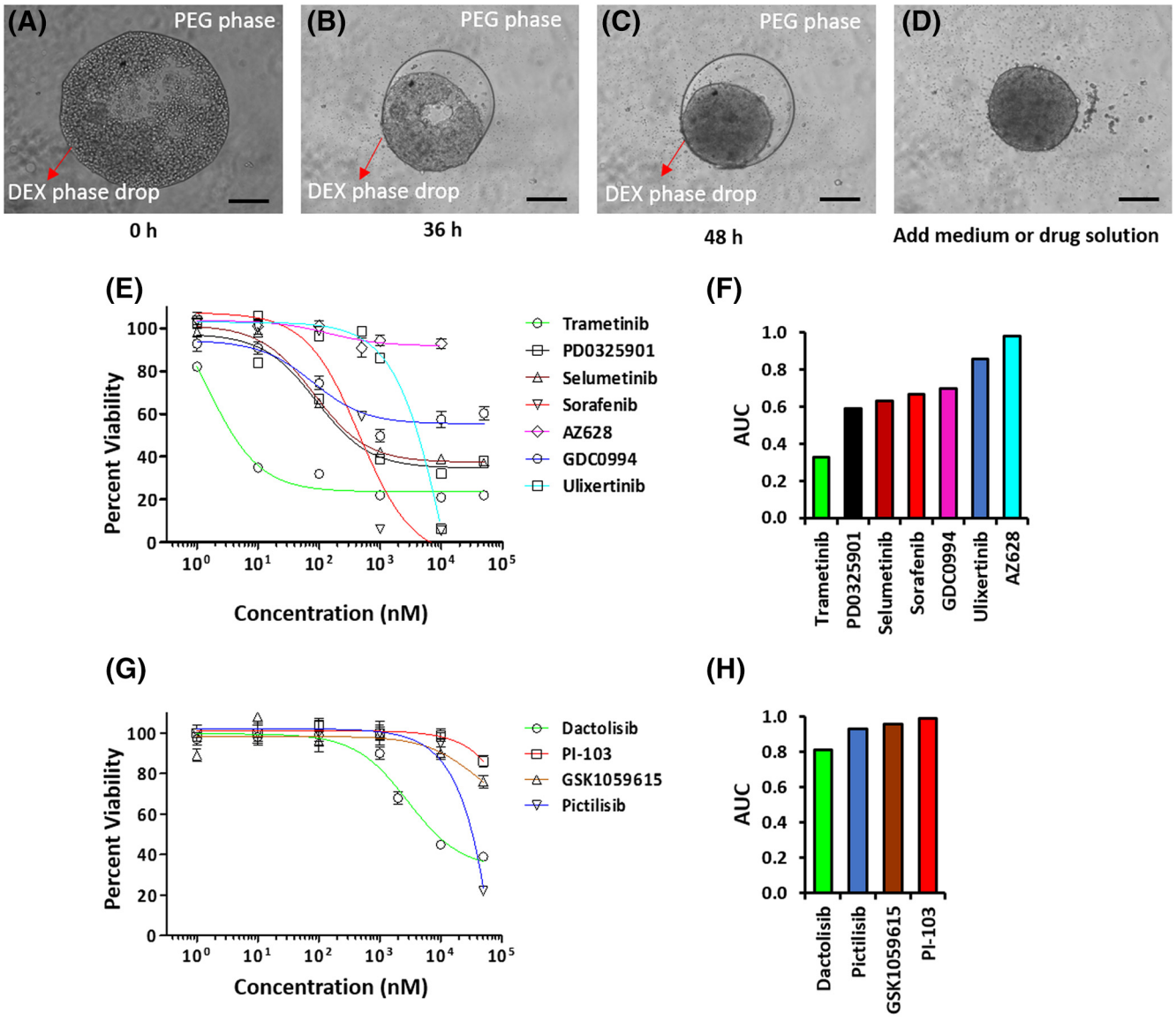

Figure 1. Tumor spheroid formation using ATPS microprinting, and screening of inhibitors of MAPK and PI3K signaling pathways against HT-29 spheroids. (A) A robotic liquid handler dispensed 0.3 μL of the aqueous DEX phase solution containing HT-29 cancer cells into a microwell containing the aqueous PEG phase. (B,C) Cancer cells remained within the nanodrop and formed a compact spheroid. (D) Addition of culture medium or a drug to the microwell diluted out the ATPS into a single medium phase containing the spheroid. (E) Dose responses of HT-29 spheroids to RAF, MEK, and ERK inhibitors. (F) Normalized AUC values from drug tests with HT-29 spheroids. (G) Dose responses of HT-29 spheroids to PI3K inhibitors. (H) Normalized AUC values from their drug tests with HT-29 spheroids. Scale bar is 200 μm.

0.2275, and– 0.0632 for the three rounds of treatment with 5 nM trametinib. The negative k_c/k_0 values during the three treatment rounds indicate that trametinib produced a cytotoxic effect. Our analysis showed that the values of k_c/k_0 during Round2 and Round3 were significantly different ($p < 0.05$) (Figure 2*E*). The average k_c/k_0 values with 100 nM PD0325901 treatment significantly increased from 0.0272 to 0.2930 and to 0.5294 for the three consecutive rounds of treatment ($p < 0.05$), respectively (Figure 2*F*). The k_c/k_0 value of Round1 treatment indicates that PD0325901 was cytostatic but this effect did not persist in subsequent treatment rounds. The average k_c/k_0 values with 100 nM selumetinib treatment also showed a significant increase from 0.1777 to 0.3231, and to 0.4745 for the three treatment rounds ($p < 0.05$) (Figure 2*G*). The k_c/k_0 values indicate that selumetinib did not generate a cytostatic effect on HT-29 cells. Overall, increasing k_c/k_0 values from Round1 to Round3 treatments with all three MEKi indicate that effects of the compounds diminished during the cyclical treatments.

To ensure that treatment-induced resistance of HT-29 spheroids to the MEKi was not limited to a single drug concentration, we performed dose-dependent tests with each MEKi and compared the normalized growth rate of spheroids treated with five different drug concentrations during Round1 and Round2. We used the IC_{50} value of each MEKi against HT-29 spheroids (Supplementary Table S3) and selected the working concentrations as multiples of the IC_{50} values. Results showed that normalized growth rates of HT-29 spheroids significantly decreased during the second treatment round at all the concentrations (Figure S2, *A-C*) ($p < 0.05$), except for treatments with trametinib at higher concentrations of 2 × IC_{50} and

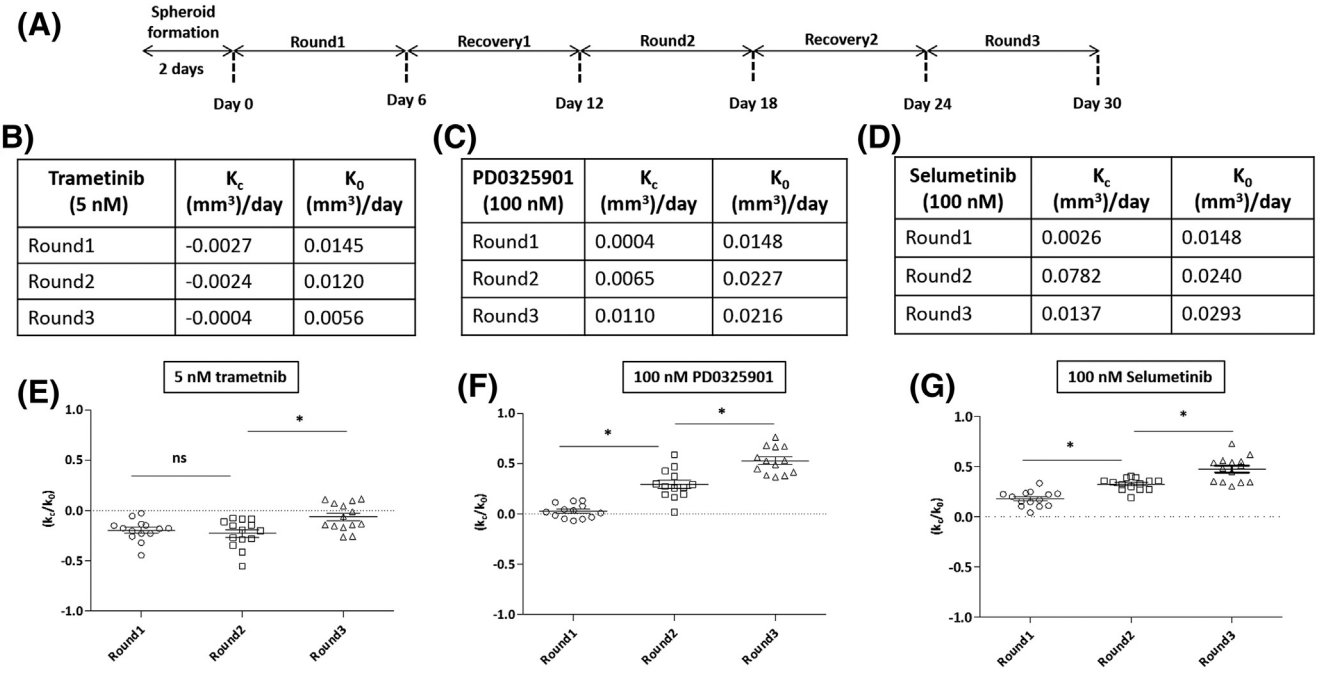

Trametinib (5 nM)	K_c (mm³)/day	K_0 (mm³)/day
Round1	-0.0027	0.0145
Round2	-0.0024	0.0120
Round3	-0.0004	0.0056

PD0325901 (100 nM)	K_c (mm³)/day	K_0 (mm³)/day
Round1	0.0004	0.0148
Round2	0.0065	0.0227
Round3	0.0110	0.0216

Selumetinib (100 nM)	K_c (mm³)/day	K_0 (mm³)/day
Round1	0.0026	0.0148
Round2	0.0782	0.0240
Round3	0.0137	0.0293

Figure 2. Cyclical drug treatment and recovery of colorectal tumor spheroids. (A) The schematic shows the experimental protocol for three cycles of treatment of HT-29 spheroids with MEKi (5 nM trametinib, 100 nM PD0325901, and 100 nM selumetinib) separated by two recovery phases. A fixed concentration of each inhibitor was used for the three treatment rounds. (B-D) Average growth rates of HT-29 spheroids during the three rounds of treatments with trametinib, PD0325901, and selumetinib, respectively. k_c was calculated as the difference in volume of drug-treated spheroids at the end and beginning of each treatment round. k_0 was calculated as the difference in volume of non-treated spheroids at the end and beginning of each round. (E-G) Quantifying resistance to MEKi treatment using a normalized growth rate (k_c/k_0) metric. n = 14 and * $p < 0.05$.

$4 \times IC_{50}$. In addition, we quantitatively compared growth rates during Round1 and Round2 under each MEKi treatment by computing the respective AUC. The results showed an increase of 1.53 folds, 3.18 folds, and 2.59 folds in AUC for treatments with trametinib, PD0325901, and selumetinib, respectively. This validated that HT-29 spheroids developed resistance to the MEKi over a wide range of concentrations.

Additionally, to validate the utility of our tumor spheroids to model treatment-induced resistance, we performed cyclical treatment and recovery of spheroids of a different colorectal cancer cell line, HCT116, with MEKi. Treatment with 5 nM trametinib significantly increased the normalized growth rate (k_c/k_0) from –0.3795 to 0.0408 and to 0.3292 during three consecutive rounds of treatment ($p < 0.05$), respectively (Figure S4*A*).

Molecular Analysis of Treatment-Induced Drug Resistance in Colorectal Tumor Spheroids

Effect of MEKi treatments on MAPK pathway activity. To elucidate molecular mechanisms of treatment-induced resistance of HT-29 spheroids to the MEKi, we first probed activity of ERK proteins because HT-29 cells have gain-of-function mutations in the MAPK pathway [7]. We found that unlike selumetinib, trametinib and PD0325901 significantly reduced ERK phosphorylation in HT-29 spheroids during treatment Round1 by 16% and 25%, respectively (Figure 3, *A* and *C*). We also investigated ERK phosphorylation in spheroids that were recovered from MEKi treatments for 6 days and found that the protein activity returned to levels comparable to those in control spheroids grown in drug-free medium for 12 days (Figure 3, *B* and *D*). Furthermore, we probed ERK activity after the second round of treatment (Round2) and found that ERK phosphorylation was significantly reduced with 5 nM trametinib and 100 nM PD0325901 treatments, but not with 100 nM selumetinib treatment (Figure 3, *G* and *H*). Thus, cells still showed transient responses to the former two inhibitors.

Effect of MEKi Treatments on PI3K Pathway Activity. Activation of PI3K pathway is a major mechanism of feedback signaling in many cancers including colorectal cancers [31–33]. We investigated whether treating HT-29 spheroids with a MEKi during Round1 augments activity of the PI3K pathway in HT-29 spheroids by probing phosphorylation of AKT. Unlike in control spheroids, treatments with all three MEKi significantly increased AKT phosphorylation in cells by 19.7, 11.4, and 12.1 folds for trametinib, PD0325901, and selumetinib, respectively (Figure 3, *A* and *E*). Shorter exposure of HT-29 spheroids to the MEKi for 48 hours also resulted in markedly higher *p*AKT than that in respective control spheroids (Figure S3). To determine whether recovery of spheroids from MEKi treatments reduces AKT activity, we quantified the *p*AKT/*t*AKT ratio at the end of Recovery1 phase. Results showed that AKT activity reduced during Recovery1 but still remained significantly higher by 2.3, 1.6, and 1.7 folds in spheroids recovered from trametinib, PD0325901, and selumetinib, respectively, than in control spheroids maintained in culture medium for 12 days (Figure 3, *B* and *F*).

To elucidate if treatment-induced feedback signaling persisted in tumor spheroids, we probed AKT activity after treatment Round2. Phosphorylation of AKT in spheroids after Round2 was significantly higher than that in spheroids that were treated during Round1, recovered (Recovery1), but did not receive any treatment during Round2 (Figure 3, *G* and *I*). This increase was 1.2, 3.6, and 1.8 folds

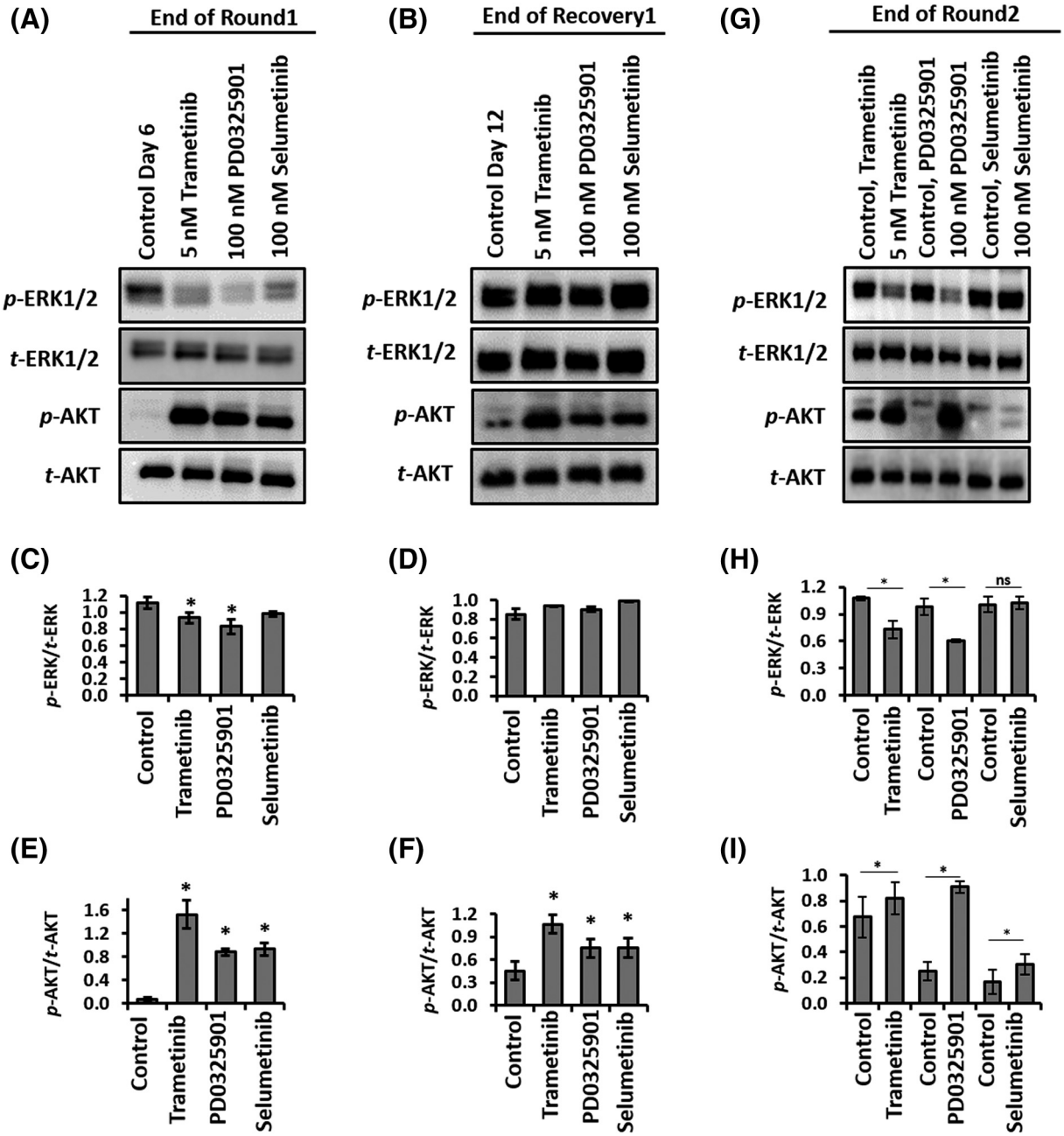

Figure 3. Oncogenic levels of ERK1/2 and AKT in HT-29 spheroids treated with MEKi. Representative Western blots for *p*-ERK1/2, *t*-ERK1/2, *p*-AKT, and *t*-AKT at end of (A) treatment Round1 phase, and at the end of (B) Recovery1 phase. (C-D) and (E-F) are quantified results of *p*-ERK/*t*-ERK, and *p*-AKT/*t*-AKT, respectively. (G) ERK1/2 and AKT levels in MEKi-treated HT-29 spheroids at the end of treatment Round2 phase. Each MEKi treatment during Round2 has different controls. **Lane 1:** Control trametinib (spheroids that received 5 nM trametinib during Round1); **Lane 2**: 5 nM trametinib treatment; **Lane 3**: Control PD0325901 (spheroids that received 100 nM PD0325901 during Round1); **Lane 4**: 100 nM PD0325901 treatment; **Lane 5**: Control selumetinib (spheroids that received 100 nM selumetinib during Round1); and **Lane 6**: 100 nM selumetinib treatment. (H) Quantified *p*-ERK/*t*-ERK showed that trametinib and PD0325901 significantly downregulated the phosphorylation of ERK, but selumetinib treatment did not significantly change ERK activity. (I) Quantified *p*-AKT/*t*-AKT showed that treatment of HT-29 spheroids with trametinib, PD0325901, and selumetinib significantly elevated AKT activity. Each experiment was repeated twice. Results are shown as mean ± standard error. * $p < 0.05$.

for treatments with trametinib, PD0325901, and selumetinib, respectively. These results suggest that MEKi treatments quickly increase AKT signaling that is sustained even when the drug is removed and when spheroids are exposed to drugs again.

As a validation step and to explore whether upregulated AKT activity due to the MEKi treatments was not limited to B-RAF mutant colorectal cancer cells, we treated spheroids of HCT116 colorectal cancer cells, which harbor KRAS mutation, with trametinib. Although trametinib treatment downregulated ERK activity in HCT116 spheroids, it induced AKT signaling (Figure S4, *B-D*). This indicates that MEKi treatment induces feedback signaling through the PI3K/AKT pathway irrespective of B-RAF or KRAS mutations in the cell lines we studied. These cell lines also harbor PIK3CA mutation. Future studies will require use of cell lines

that lack mutations in B-RAF, RAS, or PIK3CA to validate that MEKi treatment induces feedback signaling through PI3K/AKT pathway.

Effect of MEKi Treatments on B-RAF and STAT3 Signaling. It was reported that targeting MEK in colorectal cancer resulted in amplification of B-RAF, an upstream kinase of MEK, that in turn increased abundance of phosphorylated MEK and impaired the ability of selumetinib to inhibit ERK signaling [15,34]. Because we did not observe a major suppression of ERK after treatment with a MEKi, we asked whether MEKi treatments cause B-RAF amplification. Our result did not show significant changes in B-RAF activity after treatment Round1 of HT-29 spheroids with the MEKi and after the Recovery1 phase (Upper panel blots in (Figure S5, *A-B* and S5, *C-D*). Furthermore, it was shown that c-MET/STAT3 signaling mediates adaptive resistance of B-RAF mutant colorectal cancer to MEKi [11]. Therefore, we examined if treating HT-29 spheroids with the MEKi leads to the activation of this pathway. Our result showed that there was no upregulation of STAT3 kinase in the MEKi-treated spheroids after Round1 and Recovery1 phases (Lower panel blots in (Figure S5, *A-B* and S5, *E-F*).

Combination Therapy Effect on Treatment-Induced Drug Resistance

We combined each of the three MEKi with dactolisib, a potent PI3K/mTOR inhibitor, to study whether this approach could block treatment-induced resistance to MEKi in the colorectal tumor spheroids. Dactolisib was selected for the combination experiment because it was more effective that other PI3K inhibitors tested against HT-29 spheroids (Figure 1, *G-H*). We used a constant ratio approach to treat the spheroids and evaluated responses of spheroids to the treatments at the end of the six-day period, i.e., Round1, using AUC and synergism analysis [35]. The computed AUC values showed that the combination of trametinib and dactolisib was 28% and 30% more effective than the respective single-agent treatments (Figure 4*A*). We also found that the combination of PD0325901 and dactolisib enhanced the response by 36% and 41% than treatments with PD0325901 or dactolisib alone, respectively (Figure 4*B*). The combination of selumetinib and dactolisib also increased effectiveness by 15% and 18% compared to that when we used each respective inhibitor alone (Figure 4*C*). Additionally, the combination of each MEKi with dactolisib prevented growth of the spheroids and markedly reduced their size (Figure 4, *A-C*). Both trametinib/dactolisib and PD0325901/dactolisib pairs were synergistic (CI< 1) at all combinations of concentrations tested (Figure 4, *D* and *E*). Except for the 0.25 × IC_{50} concentrations pair, the selumetinib/dactolisib pair was also synergistic at all other concentrations used (Figure 4*F*). Furthermore, we determined the strength of synergism for each combination of drugs using the range of CI values shown in Table S4.

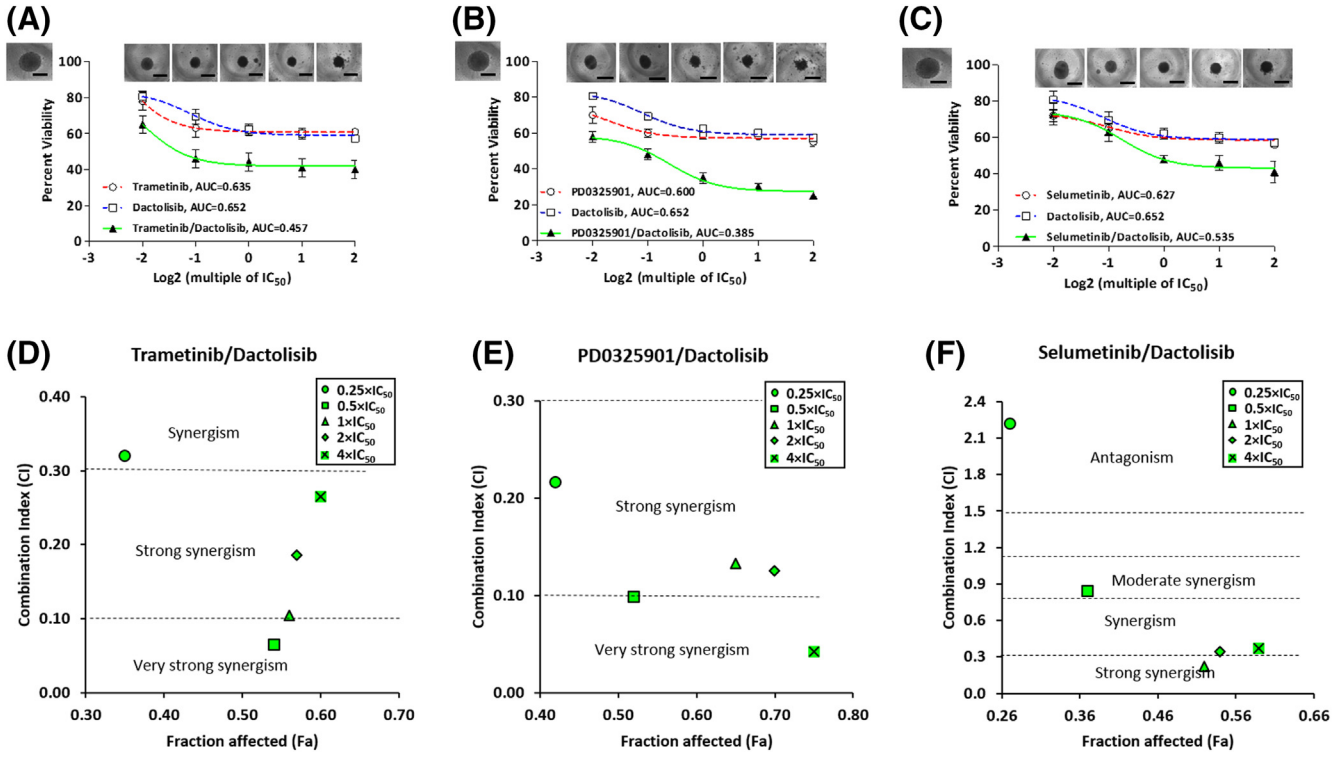

Figure 4. Combination treatments of colorectal tumor spheroids with MEKi and dactolisib. Combination and single-agent drug treatments of HT-29 spheroids with (A) trametinib and dactolisib, (B) PD0325901 and dactolisib, and (C) selumetinib and dactolisib for 6 days. Open square symbols connected by dotted blue lines represent dose-dependent responses of HT-29 spheroids to single-agent dactolisib treatments, open circle symbols connected by dotted red lines represent dose-dependent responses of HT-29 spheroids to single-agent MEKi treatments, and solid triangle symbols connected by solid green lines represent dose-dependent responses of HT-29 spheroids to combination treatments with MEKi and dactolisib. Inset images show spheroids after dose-dependent combination drug treatments. The image in the top left of panels (A-C) shows a control, non-treated spheroid. Scale bar is 300 μm. Synergy plots for the combination experiments show combination index (CI) versus fraction affected (Fa) at different combination concentrations for (D) trametinib and dactolisib, (E) PD0325901 and dactolisib, and (F) selumetinib and dactolisib. CI< 1 indicates synergism, whereas CI> 1 indicates antagonism.

Molecular Effects of Combination Treatments

We studied the effect of combination therapies with the MEKi and dactolisib to inhibit feedback signaling in colorectal tumor spheroids. We treated HT-29 spheroids with three different multiples of IC_{50} of each of the MEKi and dactolisib for 48 hours, and probed protein level activities of ERK1/2 and AKT in HT-29 spheroids. The inhibitors at these concentrations showed synergism in dose-dependent experiments (Figure 4). Table S3 shows the IC_{50} value of each inhibitor against HT-29 spheroids.

The trametinib/dactolisib pair reduced ERK activity marginally, but significantly, only at the combined IC_{50} concentrations (Figure 5, *A-B*). The inhibitors significantly reduced AKT phosphorylation dose-dependently at all three concentration pairs. The largest inhibition of AKT activity was 47% at the IC_{50} concentrations (Figure 5, *A and C*). The synergy between trametinib and dactolisib combination (Figure 4, *A* and *D*) is likely due to the downregulation of *p*-AKT, at least for the two lower combination pairs, i.e., 0.25 × IC_{50} and 0.5 × IC_{50}.

The PD0325901/dactolisib pair significantly downregulated ERK phosphorylation at the combined concentrations and in a dose-dependent manner. The largest inhibition was 98% at the combined IC_{50} concentrations (Figure 5*E*). Although this combination did not suppress AKT activity at the 0.25 × IC_{50} and 0.5 × IC_{50} concentrations, it reduced AKT phosphorylation by 24% at the combined IC_{50} concentrations (Figure 5, *D and F*). This result suggests that the synergy between these two inhibitors (Figure 5, *B* and *E*) is largely due to the downregulated ERK activity.

Selumetinib and dactolisib also significantly and dose-dependently reduced ERK phosphorylation by 58%–89% of the vehicle control (Figure 5, *G and H*). At these concentrations, AKT activity was also significantly inhibited by 52%–27% (Figure 5, *G-I*), albeit it showed an increase with increased drug concentrations. It appears that simultaneous downregulation of AKT and ERK activities facilitated the synergy between selumetinib and dactolisib (Figure 4, *C* and *F*).

Growth Inhibition of Tumor Spheroids by Long-Term Cyclic Combination Treatments

Our single-agent treatments of colorectal spheroids with MEKi activated AKT signaling. Importantly the protein activity was sustained during the long-term single-agent MEKi treatments, providing a rationale for combination therapy of the spheroids. Thus, we asked whether specific drug combinations would be effective against growth of tumor spheroids during long-term

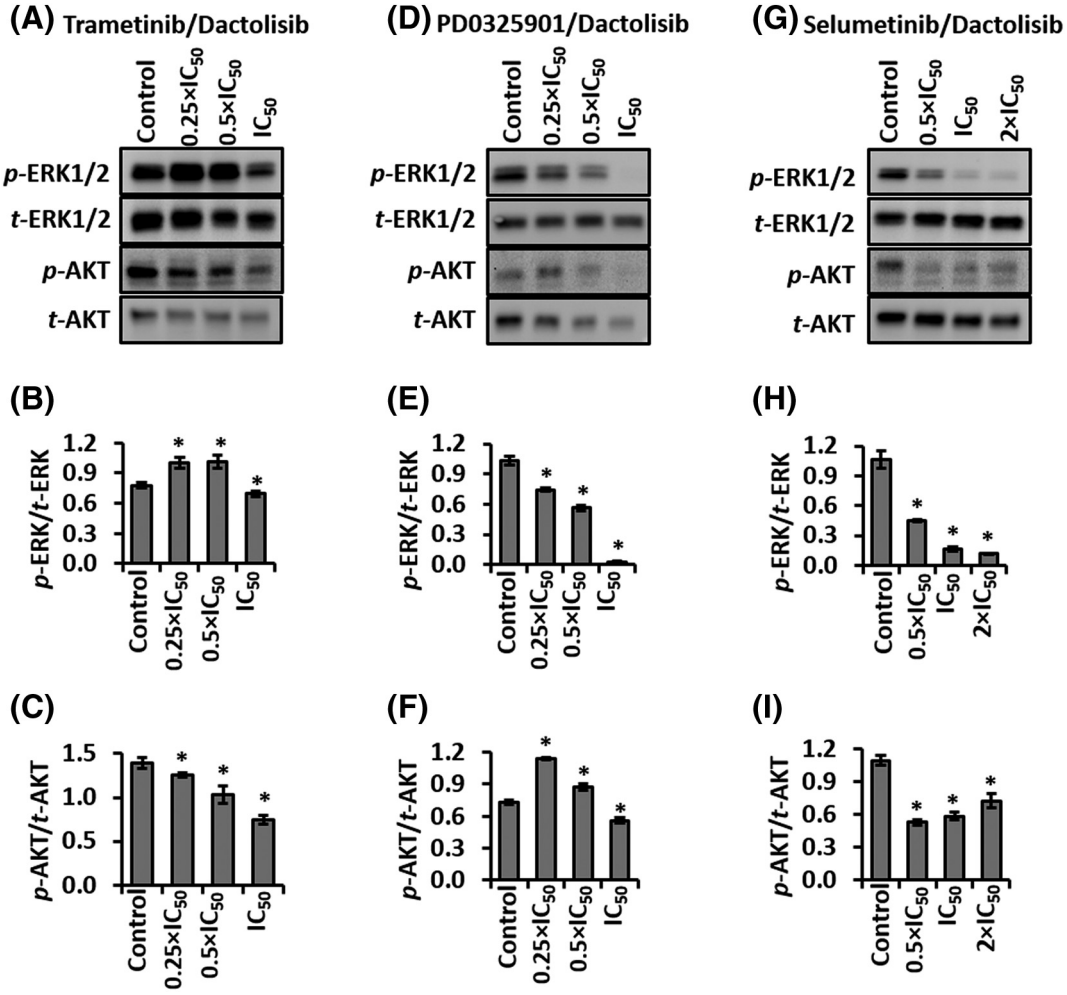

Figure 5. Combinations of MEKi and dactolisib downregulate ERK1/2 and AKT signaling in HT-29 spheroids. Representative Western blots and quantified results for *p*-ERK1/2, *t*-ERK1/2, *p*-AKT, and *t*-AKT from spheroids treated with (A-C) trametinib and dactolisib, (D-F) PD0325901 and dactolisib, and (G-I) selumetinib and dactolisib, for 48 hours. Each experiment was repeated twice. Results are shown as mean ± standard error. *$p < 0.05$ denotes comparing each treatment with its respective vehicle control.

treatment/recovery cycles (Figure 2*A*). We used the lowest synergistic concentration pairs of each of the MEKi and dactolisib, i.e., $0.25 \times IC_{50}$ for trametinib/dactolisib, $0.25 \times IC_{50}$ for PD0325901/dactolisib, and $0.5 \times IC_{50}$ for selumetinib/dactolisib to demonstrate long-term efficacy of the combination treatments. We also performed single-agent treatments with the same concentration of each inhibitor used in the respective combination treatments. In addition, we considered spheroids maintained in cell culture medium for 30 days as the vehicle control. Both the single-agent and combination treatments followed the scheme of Figure 2*A*. Comparing growth kinetics of spheroids for the vehicle control, single-agent treatments, and combination treatment in each panel of (Figure 6, *A-C*) showed that the respective combination treatment significantly delayed growth of the spheroids over the 30-day period.

To quantitatively compare efficacy of various treatments, we first calculated growth rate of spheroids as the difference in the volume of spheroids over time. Tables S5-S7 show the average values of growth rates for all the treatments and the vehicle control. Next, we calculated the growth inhibition of spheroids by each treatment as the difference in the growth rates of treated and vehicle control spheroids divided by the growth rate of the vehicle control spheroids. Among the combination treatments, the selumetinib/dactolisib pair was the most effective and inhibited the growth of HT-29 spheroids by 88%. This was followed by the PD0325901/dactolisib pair that showed a growth inhibition of 80%, and the trametinib/dactolisib pair with a 63% inhibitory effect. Figure 6, *A-C* also includes the quantified growth inhibition of all single-agent and combination treatments.

Discussion

We modeled treatment-induced resistance to MEKi by cyclically treating colorectal tumor spheroids with potent molecular inhibitors of MEK1/2 and recovering them from the treatments. Although complex mathematical approaches have been developed to model growth, transition, and dissemination dynamics in drug-sensitive and drug-resistant cancer cells [36,37], for simplicity, we used growth rate of spheroids as a metric to quantify evolving resistance of cancer cells to the MEKi in our experimental model. Several studies have demonstrated that growth of spheroids from morphological measurements closely correlates with that from biochemical analyses using MTT and Prestoblue [21,38,39]. Using morphology of spheroids to study cancer drug effects requires uniform size of spheroids prior to treatments and a consistently round shape after treatments. We

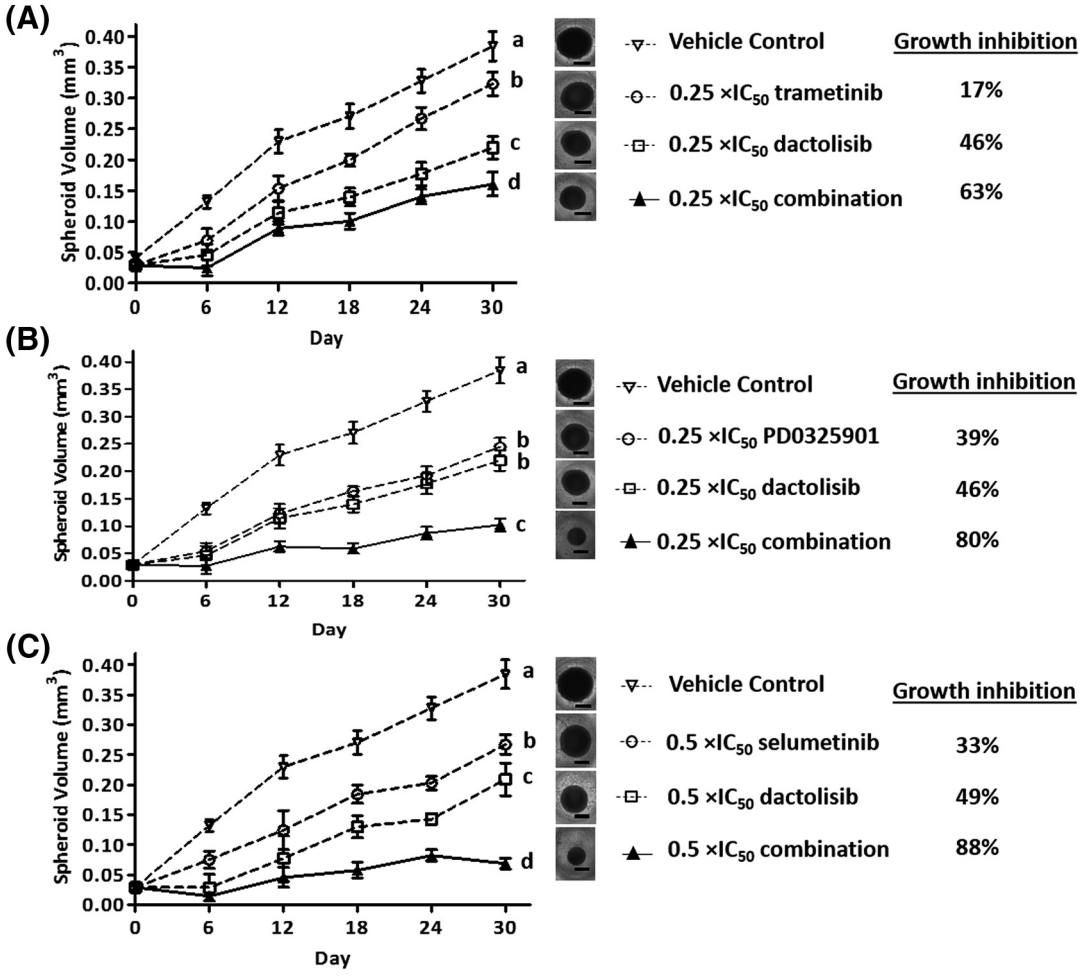

Figure 6. Long-term cyclical combination treatments. Volume of spheroids is shown during treatment and recovery cycles of Figure 2A: Vehicle control (open inverted triangles), MEKi treatment (open circles), dactolisib treatment (open squares), and combination treatment (solid triangles). All treatments were done using lowest synergistic concentrations of the MEKi and dactolisib. n = 7 and $p < 0.001$. Means of growth rates in each panel (A-C) on day 30 that do not share a letter are significantly different. Scale bar is 300 μm.

generated uniformly-sized spheroids using our aqueous two-phase microprinting technology that produces a single spheroid in each microwell and highly homogenous spheroid size distribution throughout microplates. Our previous study showed that changes in the size of spheroids over time strongly correlate with the metabolic activity of cells measured using a Prestoblue biochemical assay [21]. Therefore, we used size measurements of spheroids as a straightforward approach to determine effects of drug treatments and evolution of drug resistance in spheroids. Normalized growth rate (k_c/k_0) of spheroids takes into account changes in the size of spheroids during cycles of treatments with molecular inhibitors. We identified drug resistance of spheroids if their growth rate during a treatment cycle was significantly larger than its preceding treatment phase, i.e., $(k_c/k_0)_{i+1} > (k_c/k_0)_i$.

Our selection of molecular inhibitors of MAPK and PI3K pathways was based on selectivity of the compounds against their targets and their use in pre-clinical studies either alone or in combination therapies against colorectal cancers. The goal of our short-term screening experiments against tumor spheroids was to identify the most effective compounds and subsequently use them in long-term cyclic treatment/recovery experiments to establish that colorectal cancer cells adapt to drug treatments. Our screening identified three MEKi (trametinib, PD0325901, and selumetinib) effective against colorectal spheroids growth. The sensitivity of the colorectal cancer cells to these MEKi is consistent with studies that showed dependence of cancer cells on MEK1/2 for survival and proliferation [40], and thus, development of various MEKi to target these kinases [41]. Our quantitative study using the growth rate metric established that repeated use of MEKi induces resistance in colorectal tumor spheroids independent of drug concentration (Figures 2, S1 and S2). Our result is consistent with in vivo studies that showed cyclic treatment of tumor xenografts with MEKi did not reduce tumor size [42,43], thereby necessitating alternative treatments.

Our molecular analysis showed that trametinib and PD0325901 only moderately downregulated ERK phosphorylation during the first round of treatment, despite specificity of these MEKi toward their target. We suspect that the moderate effects of these MEKi was due to their low concentrations used in our experiments (Figure 3, *A* and *C*). Our previous study using a higher trametinib concentration (100 nM) showed complete inhibition of ERK activity in HT-29 spheroids [21]. Despite moderate effects of these compounds, ERK phosphorylation fully recovered during the recovery phase (Figure 3, *B* and *D*), indicating that the MEKi produce a transient response in the cancer cells. Gain of ERK activity during the recovery phase allowed the colorectal tumor spheroids to show sensitivity to the MEKi during the second round of treatments with trametinib and PD0325901 (Figure 3, *G* and *H*). The inability of selumetinib to downregulate ERK signaling during subsequent treatment rounds was likely a reason for the increase in growth rate and resistance of colorectal tumor spheroids to this compound.

Inhibition of MEK has been reported to reactivate PI3K signaling, motivating us to investigate signaling through AKT as a mechanism of resistance to cyclical therapy [32,44]. Our results showed that only 48 hours of exposure of HT-29 spheroids to a MEKi elevated AKT phosphorylation (Figure S3). The *p*-AKT levels were significantly high during Round1 treatments with a MEKi (Figure 3*E*). Phosphorylated AKT remained significantly increased even after removing drugs during the Recovery1 phase (Figure 3*F*) and following exposure of spheroids to a MEKi during Round2 (Figure 3*I*). Our validation of this phenomenon with spheroids of KRAS-mutant HCT116 cells indicates that MEKi-induced activation of PI3K/AKT/mTOR pathway is a major mechanism of feedback signaling in colorectal cancer cells that we have studied. Our results are consistent with other reports that showed phosphorylation of AKT in various RAF- and RAS-mutant lung and colorectal cancer cells under RAFi or MEKi treatments [45,46], and in a genetically engineered Apc- and KRAS-mutant colorectal cancer mouse model under MEK162 treatment [47]. On the other hand, several studies also showed that treatment with a MEKi (selumetinib) induced amplification of B-RAF, which in turn reduced the efficacy of the MEKi to inhibit ERK [15,34]. Additionally, MEKi treatments activated c-MET/STAT3 signaling in BRAF-mutant colorectal cancer models both in vitro and in vivo [11]. However, we did not observe amplification of B-RAF or activation of STAT3 (Figure S5), confirming that compensatory AKT signaling in colorectal HT-29 tumor spheroids is the main mechanism of acquired resistance to the MEKi. Morphologically, this adaptive resistance was evident from increases in the growth rate of spheroids under single-agent treatments with MEKi (Figure S1, *G-I*).

We successfully blocked this feedback signaling by combining a MEKi and dactolisib and showed that all the combinations synergistically inhibited growth of HT-29 spheroids and downregulated phosphorylation of both ERK and AKT when we used sufficiently high concentrations of the compounds. Importantly, parallel inhibition of MAPK and PI3K pathways resulted in suppression of growth of spheroids during long-term combination MEKi and dactolisib treatments. We demonstrated that long-term cyclic treatments of colorectal tumor spheroids with combinations of MEKi and dactolisib effectively prevented growth of the spheroids by as high as 88% compared to the non-treated vehicle controls. We achieved this improved activity at significantly lower doses of MEKi and dactolisib, an effect that was significantly greater than that with either single-agent treatment at the same drug concentration. Although clinical trial combining MAPK and PI3K inhibitors has been unsuccessful because of toxicity [48], using a lower concentration of each compound or temporal changes in dosing such as in cyclic treatments may help reduce toxicity. Our 3D resistance model enables high throughput testing of different drug combinations over a wide concentration range to select effective pairs of drugs at optimal doses and also allows testing different treatment regimens to identify those with reduced toxicity than dual combination treatments.

Our results are consistent with studies that showed intermittent/cyclic dosing of MEKi with PI3K inhibitors significantly suppresses growth of tumors in animal models. For example, the MEKi GDC-0943 exhibited synergy with the PI3K inhibitor GDC-0941 by inhibiting tumor growth and inducing apoptosis in DLD-1 colorectal tumor xenografts [42]. Similarly, the MEKi PD0325901 exhibited synergy with the PI3K inhibitor GDC-0941 in non-small cell lung cancer xenografts [43], and HCT116 and HT-29 colorectal xenografts [49]. Our findings are also in agreement with previous reports that MEKi and PI3K/mTOR inhibitor combinations generated anti-proliferative effects in colorectal cancer cells by reducing ERK, AKT, and S6 activities [42,45,50,51]. Prior intermittent dosing studies showed prolonged effects on downstream markers of proliferation and apoptosis [42,43], which may be responsible for significantly reduced growth of colorectal tumor spheroids under combination therapies in our long-term treatment studies. Therefore, a significant aspect of our study is the use of a 3D

in vitro colorectal tumor model in cyclic treatment and recovery with molecular inhibitors to reliably emulate results in animal models. But unlike time-consuming patient-derived xenograft (PDX) models, our approach enables convenient high throughput testing of various drug combinations to identify promising treatments. Incorporating our model in mainstream anti-cancer drug screening will save time and cost, accelerating drug discovery and development.

In conclusion, this study presented a novel model of cyclic drug treatment and recovery of tumor spheroids to demonstrate that single-agent treatments with targeted kinase inhibitors leads to adaptive drug resistance of cancer cells. The utility of our spheroid technology to model treatment-induced resistance of colorectal cancer cells coupled with a comprehensive molecular analysis identified molecular makers of resistance and helped rationally design combination treatments that effectively blocked growth of tumor spheroids. Our 3D resistance model will advance mechanistic understanding of drug resistance in different cancers and testing of therapeutics and different regimens to overcome resistance with reduced toxicity. Furthermore, the use of this model with patient-derived cells of different genetic signatures may offer a major precision medicine tool to improve treatment outcomes.

Conflicts of Interest

Authors declare no conflict of interest.

Authors' Contributions

Concept and design: P. Shahi Thakuri, H. Tavana; Development and methodology: P. Shahi Thakuri, H. Tavana; Acquisition, analysis and interpretation of data: P. Shahi Thakuri, G.D. Luker, H. Tavana; Writing, review, and/or revision of the manuscript: P. Shahi Thakuri, G.D. Luker, H. Tavana; Study supervision: H. Tavana.

Acknowledgement

Financial support was provided by a grant, R15CA216413, from the National Institutes of Health.

Appendix A. Supplementary data

Supplementary data to this article can be found online at https://doi.org/10.1016/j.tranon.2018.11.009.

References

[1] Waring MJ, Arrowsmith J, Leach AR, Leeson PD, Mandrell S, Owen RM, Pairaudeau G, Pennie WD, Pickett SD, and Wang J, et al (2015). An analysis of the attrition of drug candidates from four major pharmaceutical companies. *Nat Rev Drug Discov* **14**, 475–486.

[2] Ham SL, Joshi R, Thakuri PS, and Tavana H (2016). Liquid-based three-dimensional tumor models for cancer research and drug discovery. *Exp Biol Med* **241**, 939–954.

[3] Shahi Thakuri P, Liu C, Luker GD, and Tavana H (2017). Biomaterials-based approaches to tumor spheroid and organoid modeling. *Adv Healthc Mater* 7e1700980.

[4] Thoma CR, Zimmermann M, Agarkova I, Kelm JM, and Krek W (2014). 3D cell culture systems modeling tumor growth determinants in cancer target discovery. *Adv Drug Deliv Rev* **69–70**, 29–41.

[5] Siegel R, DeSantis C, and Jemal A (2014). Colorectal cancer statistics, 2014. *CA Cancer J Clin* **64**, 104–117.

[6] Liu X, Jakubowski M, and Hunt JL (2011). KRAS gene mutation in colorectal cancer is correlated with increased proliferation and spontaneous apoptosis. *Am J Clin Pathol* **135**, 245–252.

[7] Davies H, Bignell GR, Cox C, Stephens P, Edkins S, Clegg S, Teague J, Woffendin H, Garnett MJ, and Bottomley W, et al (2002). Mutations of the BRAF gene in human cancer. *Nature* **417**, 949–954.

[8] Mei ZB, Duan CY, Li CB, Cui L, and Ogino S (2016). Prognostic role of tumor PIK3CA mutation in colorectal cancer: a systematic review and meta-analysis. *Ann Oncol* **27**, 1836–1848.

[9] Sebolt-Leopold JS, Dudley DT, Herrera R, Van Becelaere K, Wiland A, Gowan RC, Tecle H, Barret SD, Bridges A, and Przybranowski S, et al (1999). Blockade of the MAP kinase pathway suppresses growth of colon tumors in vivo. *Nat Med* **5**, 810–816.

[10] Yang H, Higgins B, Kolinsky K, Packman K, Bradley WD, Lee RJ, Schostack K, Simcox ME, Kopetz S, and Hemibrook D, et al (2012). Antitumor activity of BRAF inhibitor vemurafenib in preclinical models of BRAF-mutant colorectal cancer. *Cancer Res* **72**, 779–789.

[11] Carson R, Celtikci B, Fenning C, Javadi A, Crawford N, Carbonell LP, Lawler M, Longley DB, Johnston PG, and Van Schaeybroecket S (2015). HDAC Inhibition Overcomes Acute Resistance to MEK Inhibition in BRAF-Mutant Colorectal Cancer by Downregulation of c-FLIPL. *Clin Cancer Res* **21**, 3230–3240.

[12] Corcoran RB, Ebi H, Turke AB, Coffee EM, Nishino M, Cogdill AP, Brown RD, Della Pelle P, Dias-Santagata D, and Hung KE, et al (2012). EGFR-mediated re-activation of MAPK signaling contributes to insensitivity of BRAF mutant colorectal cancers to RAF inhibition with vemurafenib. *Cancer Discov* **2**, 227–235.

[13] Wang H, Daouti S, Li W-H, Wen Y, Rizzo C, Higgins B, Packman K, Rosen N, Boylan JF, and Heimbrook D, et al (2011). Identification of the MEK1(F129L) activating mutation as a potential mechanism of acquired resistance to MEK inhibition in human cancers carrying the B-RafV600E mutation. *Cancer Res* **71**, 5535–5545.

[14] Ahronian LG, Sennott EM, Van Allen EM, Wagle N, Kwak EL, Faris JE, Godfrey JT, Nishimura K, Lynch KD, and Mermel CH, et al (2015). Clinical acquired resistance to RAF inhibitor combinations in BRAF-mutant colorectal cancer through MAPK pathway alterations. *Cancer Discov* **5**, 358–367.

[15] Corcoran RB, Dias-Santagata D, Bergethon K, Iafrate AJ, Settleman J, and Engelman JA (2010). BRAF gene amplification can promote acquired resistance to MEK inhibitors in cancer cells harboring the BRAF V600E mutation. *Sci Signal* **3**, ra84.

[16] Spugnini EP, Dragonetti E, Vincenzi B, Onori N, Citro G, and Baldi A (2006). Pulse-mediated chemotherapy enhances local control and survival in a spontaneous canine model of primary mucosal melanoma. *Melanoma Res* **16**, 23–27.

[17] Solit DB, She Y, Lobo J, Kris MG, Scher HI, Rosen N, and Sirotnak FM (2005). Pulsatile administration of the epidermal growth factor receptor inhibitor gefitinib is significantly more effective than continuous dosing for sensitizing tumors to paclitaxel. *Clin Cancer Res* **11**, 1983–1989.

[18] Rimawi MF, Wiechmann LS, Wang Y-C, Huang C, Migliaccio I, Wu M-F, Gutierrez C, Hilsenbeck SG, Arpino G, and Massarweh S, et al (2011). Reduced dose and intermittent treatment with lapatinib and trastuzumab for potent blockade of the HER pathway in HER2/neu-overexpressing breast tumor xenografts. *Clin Cancer Res* **17**, 1351–1361.

[19] Das Thakur M, Salangsang F, Landman AS, Sellers WR, Pryer NK, Levesque MP, Dummer R, McMahon M, and Stuart DD (2013). Modelling vemurafenib resistance in melanoma reveals a strategy to forestall drug resistance. *Nature* **494**, 251–255.

[20] Bennouna J, Sastre J, Arnold D, Österlund P, Greil R, Van Cutsem E, von Moos R, Viéitez JM, Bouché O, and Borg C, et al (2013). Continuation of bevacizumab after first progression in metastatic colorectal cancer (ML18147): a randomised phase 3 trial. *Lancet Oncol* **14**, 29–37.

[21] Shahi Thakuri P, Ham SL, Luker GD, and Tavana H (2016). Multiparametric analysis of oncology drug screening with aqueous two-phase tumor spheroids. *Mol Pharm* **13**, 3724–3735.

[22] Shahi Thakuri P and Tavana H (2017). Single and combination drug screening with aqueous biphasic tumor spheroids. *SLAS Discov* **22**, 507–515.

[23] Atefi E, Lemmo S, Fyffe D, Luker GD, and Tavana H (2014). High throughput, polymeric aqueous two-phase printing of tumor spheroids. *Adv Funct Mater* **24**, 6509–6515.

[24] Lemmo S, Atefi E, Luker GD, and Tavana H (2014). Optimization of aqueous biphasic tumor spheroid microtechnology for anti-cancer drug testing in 3D culture. *Cell Mol Bioeng* **7**, 344–354.

[25] Atefi E, Fyffe D, Kaylan KB, and Tavana H (2016). Characterization of aqueous two-phase systems from volume and density measurements. *J Chem Eng Data* **61**, 1531–1539.

[26] Ham SL, Joshi R, Luker GD, and Tavana H (2016). Engineered breast cancer cell spheroids reproduce biologic properties of solid tumors. *Adv Healthc Mater* **5**, 2788–2798.

[27] Ahmed D, Eide PW, Eilertsen IA, Danielsen SA, Eknæs M, Hektoen M, Lind GE, and Lothe RA (2013). Epigenetic and genetic features of 24 colon cancer cell lines. *Oncogene* **2**e71.
[28] Fang JY and Richardson BC (2005). The MAPK signalling pathways and colorectal cancer. *Lancet Oncol* **6**, 322–327.
[29] Engelman JA (2009). Targeting PI3K signalling in cancer: opportunities, challenges and limitations. *Nat Rev Cancer* **9**, 550–562.
[30] De Roock W, De Vriendt V, Normanno N, Ciardiello F, and Tejpar S (2011). KRAS, BRAF, PIK3CA, and PTEN mutations: implications for targeted therapies in metastatic colorectal cancer. *Lancet Oncol* **12**, 594–603.
[31] Balmanno K, Chell SD, Gillings AS, Hayat S, and Cook SJ (2009). Intrinsic resistance to the MEK1/2 inhibitor AZD6244 (ARRY-142886) is associated with weak ERK1/2 signalling and/or strong PI3K signalling in colorectal cancer cell lines. *Int J Cancer* **125**, 2332–2341.
[32] Turke AB, Song Y, Costa C, Cook R, Arteaga CL, Asara JM, and Engelman JA (2012). MEK inhibition leads to PI3K/AKT activation by relieving a negative feedback on ERBB receptors. *Cancer Res* **72**, 3228–3237.
[33] Mirzoeva OK, Collisson EA, Schaefer PM, Hann B, Hom YK, Ko AH, and Korn WM (2013). Subtype-specific MEK-PI3 kinase feedback as a therapeutic target in pancreatic adenocarcinoma. *Mol Cancer Ther* **12**, 2213–2225.
[34] Little AS, Balmanno K, Sale MJ, Newman S, Dry JR, Hampson M, Edwards PA, Smith PD, and Cook SJ (2011). Amplification of the driving oncogene, KRAS or BRAF, underpins acquired resistance to MEK1/2 inhibitors in colorectal cancer cells. *Sci Signal* **4**ra17.
[35] Chou T-C (2010). Drug combination studies and their synergy quantification using the Chou-Talalay method. *Cancer Res* **70**, 440–446.
[36] Sun X, Bao J, and Shao Y (2016). Mathematical modeling of therapy-induced cancer drug resistance: connecting cancer mechanisms to population survival rates. *Sci Rep* **6**22498.
[37] Foo J and Michor F (2009). Evolution of resistance to targeted anti-cancer therapies during continuous and pulsed administration strategies. *PLoS Comput Biol* **5**e1000557.
[38] Ivanov DP, Parker TL, Walker DA, Alexander C, Ashford MB, Gellert PR, and Garnett MC (2014). Multiplexing spheroid volume, resazurin and acid phosphatase viability assays for high-throughput screening of tumour spheroids and stem cell neurospheres. *PLoS One* **9**e103817.
[39] Vinci M, Gowan S, Boxall F, Patterson L, Zimmermann M, Court W, Lomas C, Mendiola M, Hardisson D, and Eccles SA (2012). Advances in establishment and analysis of three-dimensional tumor spheroid-based functional assays for target validation and drug evaluation. *BMC Biol* **10**, 10–29.
[40] Dhillon AS, Hagan S, Rath O, and Kolch W (2007). MAP kinase signalling pathways in cancer. *Oncogene* **26**, 3279–3290.
[41] Caunt CJ, Sale MJ, Smith PD, and Cook SJ (2015). MEK1 and MEK2 inhibitors and cancer therapy: the long and winding road. *Nat Rev Cancer* **15**, 577–592.
[42] Hoeflich KP, Merchant M, Orr C, Chan J, Den Otter D, Berry L, Kasman I, Koeppen H, Rice K, and Yang NY, et al (2012). Intermittent administration of MEK inhibitor GDC-0973 plus PI3K inhibitor GDC-0941 triggers robust apoptosis and tumor growth inhibition. *Cancer Res* **72**, 210–219.
[43] Sos ML, Fischer S, Ullrich R, Peifer M, Heuckmann JM, Koker M, Heynck S, Stückrath I, Weiss J, and Fischer F, et al (2009). Identifying genotype-dependent efficacy of single and combined PI3K- and MAPK-pathway inhibition in cancer. *Proc Natl Acad Sci* **106**, 18351–18356.
[44] Mirzoeva OK, Das D, Heiser LM, Bhattacharya S, Siwak D, Gendelman R, Bayani N, Wang NJ, Neve RM, and Guan Y, et al (2009). Basal subtype and MAPK/ERK kinase (MEK)-phosphoinositide 3-kinase feedback signaling determine susceptibility of breast cancer cells to MEK inhibition. *Cancer Res* **69**, 565–572.
[45] Haagensen EJ, Kyle S, Beale GS, Maxwell RJ, and Newell DR (2012). The synergistic interaction of MEK and PI3K inhibitors is modulated by mTOR inhibition. *Br J Cancer* **106**, 1386–1394.
[46] Manchado E, Weissmueller S, Morris JP, Chen C-C, Wullenkord R, Lujambio A, de Stanchina E, Poirier JT, Gainor JF, and Corcoran RB, et al (2016). A combinatorial strategy for treating KRAS-mutant lung cancer. *Nature* **534**, 647–651.
[47] Raja M, Zverev M, Seipel K, Williams GT, Clarke AR, and Shaw PHS (2015). Assessment of the in vivo activity of PI3K and MEK inhibitors in genetically defined models of colorectal cancer. *Mol Cancer Ther* **14**, 2175–2186.
[48] Shimizu T, Tolcher AW, Papadopoulos KP, Beeram M, Rasco DW, and Smith LS, et al (2012). The clinical effect of the dual-targeting strategy involving PI3K/AKT/mTOR and RAS/MEK/ERK pathways in patients with advanced cancer. *Clin Cancer Res* **18**, 2316–2325.
[49] Haagensen EJ, Thomas HD, Wilson I, Harnor SJ, Payne SL, Rennison T, Smith KM, Maxwell RJ, and Newell DR (2013). The enhanced in vivo activity of the combination of a MEK and a PI3K inhibitor correlates with [18F]-FLT PET in human colorectal cancer xenograft tumour-bearing mice. *PLoS One* **8**e81763.
[50] Kinross KM, Brown DV, Kleinschmidt M, Jackson S, Christensen J, Cullinane C, Hicks RJ, Johnstone RJ, and McArthur GA (2011). In vivo activity of combined PI3K/mTOR and MEK inhibition in a KrasG12D; Pten deletion mouse model of ovarian cancer. *Mol Cancer Ther* **10**, 1440–1449.
[51] Pitts TM, Newton TP, Bradshaw-Pierce EL, Addison R, Arcaroli JJ, Klauck PJ, Bagby SM, Hyatt SL, Purkey A, and Tentler JJ, et al (2014). Dual pharmacological targeting of the MAP kinase and PI3K/mTOR pathway in preclinical models of colorectal cancer. *PLoS One* **9**e113037.